Clim. Past Discuss., 8, 4663–4699, 2012
www.clim-past-discuss.net/8/4663/2012/
doi:10.5194/cpd-8-4663-2012

Climate of the Past Discussions

Last interglacial temperature evolution – a model inter-comparison

P. Bakker[1], E. J. Stone[2], S. Charbit[3], M. Gröger[4], U. Krebs-Kanzow[5], S. P. Ritz[6], V. Varma[7], S. Khon[5], D. J. Lunt[2], U. Mikolajewicz[4], M. Prange[7], H. Renssen[1], B. Schneider[5], and M. Schulz[7]

[1]Earth & Climate Cluster, Department of Earth Sciences, VU University Amsterdam, 1081HV Amsterdam, The Netherlands
[2]Bristol Research Initiative for the Dynamic Global Environment (BRIDGE), School of Geographical Sciences, University of Bristol, Bristol BS8 1SS, UK
[3]LSCE-CEA-CNRS, Laboratoire des Sciences du climat et de l'environnement (IPSL/LSCE), UMR CEA-CNRS-UVSQ8212, CE-Saclay, Orme des Merisiers, 91191 Gif sur Yvette, France
[4]Max Planck Institute for Meteorology, Bundesstrasse 53, 20146 Hamburg, Germany
[5]Institute for Geosciences, Kiel University, Ludewig-Meyn-Str. 10, 24118 Kiel, Germany
[6]Climate and Environmental Physics, Physics Institute, and Oeschger Centre for Climate Change Research, University of Bern, Bern, Switzerland
[7]MARUM – Center for Marine Environmental Sciences and Faculty of Geosciences, University of Bremen, Klagenfurter Strasse, 28334 Bremen, Germany

Received: 16 July 2012 – Accepted: 31 July 2012 – Published: 20 September 2012

Correspondence to: P. Bakker (p.bakker@vu.nl)

Published by Copernicus Publications on behalf of the European Geosciences Union.

CPD
8, 4663–4699, 2012

Abstract

There is a growing number of proxy-based reconstructions detailing the climatic changes during the Last Interglacial period. This period is of special interest because large parts of the globe were characterized by a warmer-than-present-day climate, making this period an interesting test bed for climate models in the light of projected global warming. However, mainly because synchronizing the different records is difficult, there is no consensus on a global picture of Last Interglacial temperature changes. Here we present the first model inter-comparison of transient simulations covering the Last Interglacial period. By comparing the different simulations we aim at investigating the robustness of the simulated surface air temperature evolution.

The model inter-comparison shows a robust Northern Hemisphere July temperature evolution characterized by a maximum between 130–122 ka BP with temperatures 0.4 to 6.8 K above pre-industrial values. This temperature evolution is in line with the changes in June insolation and greenhouse-gas concentrations. For the evolution of July temperatures in the Southern Hemisphere, the picture emerging from the inter-comparison is less clear. However, it does show that including greenhouse-gas concentration changes is critical. The simulations that include this forcing show an early, 128 ka BP July temperature anomaly maximum of 0.5 to 2.6 K. The robustness of simulated January temperatures is large in the Southern Hemisphere and the mid-latitudes of the Northern Hemisphere. In these latitudes maximum January temperature anomalies of respectively −2.5 to 2 K and 0 to 2 K are simulated for the period after 118 ka BP. The inter-comparison is inconclusive on the evolution of January temperatures in the high-latitudes of the Northern Hemisphere.

Further investigation of regional anomalous patterns and inter-model differences indicate that in specific regions, feedbacks within the climate system are important for the simulated temperature evolution. Firstly in the Arctic region, changes in the summer sea-ice cover control the evolution of Last Interglacial winter temperatures. Secondly, for the Atlantic region, the Southern Ocean and the North Pacific, possible changes

CPD
8, 4663–4699, 2012

in the characteristics of the Atlantic meridional overturning circulation are critical. The third important feedback, having an impact on the temperature evolution of the Northern Hemisphere, is shown to be the presence of remnant continental ice from the preceding glacial period. Another important feedback are changes in the monsoon regime which controls the evolution of temperatures over parts of Africa and India. Finally, the simulations reveal an important land-sea contrast, with temperature changes over the oceans lagging continental temperatures by up to several thousand years. The aforementioned feedback mechanisms tend to be highly model-dependent, indicating that specific proxy-data is needed to constrain future climate simulations and to further enhance our understanding of the evolution of the climate during the Last Interglacial period.

1 Introduction

To strengthen our confidence in climate models, it is important to assess their ability to realistically simulate a climate different from the present-day climate (Braconnot et al., 2012). The Last Interglacial Period (LIG; ~ 130 000–115 000 yr BP) provides an interesting period because many proxy-based reconstructions show temperatures up to several degrees higher than present-day (CAPE-members, 2006; Turney and Jones, 2010; McKay et al., 2011). However, to date, the evolution of the climate during the LIG is still under debate. This is especially true for the establishment of peak interglacial warmth in different regions. For instance, proxy-based reconstruction of surface temperatures from the Norwegian Sea and the North Atlantic are inconclusive on whether peak interglacial warmth occurred in the first or in the second part of the LIG (Bauch and Kandiano, 2007; Nieuwenhove et al., 2011; Govin et al., 2012). The main cause of this uncertainty is the difficulty to establish a coherent stratigraphic framework for the LIG period, not only between different regions (e.g. the Norwegian Sea and the North Atlantic) but also between different types of proxy-archives (e.g. speleothems, ice cores, deep-sea cores and lake sediments, e.g. Waelbroeck et al., 2008). Deciphering

CPD
8, 4663–4699, 2012

the evolution of LIG surface temperatures is further complicated by the fact that different types of proxies record different parts of the climatic signal: for instance maximum summer warmth, the number of days above a threshold temperature, the seasonal temperature contrast or average summer temperatures (Jones and Mann, 2002; Sirocko et al., 2006). Climate simulations covering the LIG period can be used to facilitate the interpretation of proxy-based temperature reconstructions by providing information on the timing of peak interglacial warmth for different months and on possible spatial differences in the evolution of temperatures.

For the LIG period a large number of equilibrium simulations have been analysed (Montoya, 2007; Lunt et al., 2012, and references therein). However, to investigate the evolution of temperatures throughout this period and the timing of maximum warmth (MWT), the transient nature of two of the major forcings, changes in the astronomical configuration and changes in the concentrations of the major greenhouse-gases (GHGs), have to be incorporated. So far only a small number of transient climate simulations have been performed for the LIG (e.g. Crucifix and Berger, 2002; Calov et al., 2005; Gröger et al., 2007; Ritz et al., 2011a). However, the simulated temperature evolution is highly model-dependent. In order to investigate the robustness of the results of individual climate simulations, we have performed the first model inter-comparison study of long, $>10\,000$ yr, transient simulations covering the LIG period. This inter-comparison includes both published LIG transient simulations (Gröger et al., 2007) as well as ones recently performed within the PMIP3 framework (Paleoclimate Modelling Intercomparison Project).

In line with the majority of available proxy-based climate reconstructions, we have restricted the model inter-comparison to surface air temperatures. The objectives of this model inter-comparison are: (1) to evaluate the robustness of the transient temperature response to LIG forcings in the different models and (2) to analyse the simulated spatio-temporal response of temperatures during the LIG. The climate models used in this inter-comparison study differ in complexity from 2.5-D-atmosphere-ocean-vegetation models to General-Circulation-Models (GCMs). Some also differ in terms of

CPD
8, 4663–4699, 2012

the climate forcings used (Table 1). This enables us to perform a first investigation of the importance of modelcomplexity and different forcings. Finally, in the discussion we will describe specific spatial and temporal patterns in simulated temperatures which indicate that several major climatic feedbacks, linked to sea-ice, the Atlantic meridional overturning circulation (AMOC), remnant ice sheets from the last glacial period, the monsoon and land-sea contrasts, are important in determining the evolution of LIG temperatures. This study provides an important step towards a future comparison of LIG proxy-based reconstructions and transient model simulations.

2 Model simulations

We performed transient LIG climate simulations with a total of 7 different climate models of different complexity. In this section we describe the main characteristics of the models and the performed simulations (for details see Table 1). For a more thorough description of the different models the reader is referred to the original articles. In the second part of this section, an overview of the evolution of the main climate forcings of the LIG period is given in terms of: the changes in the insolation received by the Earth and the changes in the GHG concentrations.

2.1 Description of the climate models

2.1.1 Bern3D

The Bern3D Earth system model of intermediate complexity (EMIC) consists of a two-dimensional atmospheric energy and moisture balance model that is coupled to a three-dimensional sea-ice-ocean model. In the atmospheric component, heat is transported horizontally by diffusion only while moisture is transported by both diffusion and prescribed advection (Edwards and Marsh, 2005; Müller et al., 2006; Ritz et al., 2011a,b). This means that, compared to other models, the spatial and temporal changes in surface temperatures simulated by the Bern3D model are more directly

CPD
8, 4663–4699, 2012

linked to local changes in the radiative forcing. The model includes prescribed changes in the extent of the Northern Hemisphere (NH) continental ice sheets (the Antarctic ice sheet is fixed to present-day configuration due to the coarse resolution of the model at high latitudes). The extent of the NH continental ice sheets is calculated using the benthic δ^{18}O stack (a proxy for global ice volume) of Lisiecki and Raymo (2005) in order to scale the ice sheets extent between the modern and the Last Glacial Maximum extent (Ritz et al., 2011a). Consequently, remnant ice from the preceding glacial period is prescribed until ~ 125 ka BP, while a present-day extent is prescribed between ~ 125 ka–121 ka BP after which the extent of the NH continental ice sheets starts to increase again. Related to a decrease of the extent of the ice sheet, the model includes a meltwater flux from the melting remnant ice sheets into the ocean. During the period when the ice sheets increase, freshwater is removed globally from the ocean surface. The Bern3D transient LIG simulation used in this study is part of a longer run spanning several glacial cycles. The simulation is similar to the one presented by Ritz et al. (2011a) but with the adjusted parameter set of Ritz et al. (2011b). Because of this, combined with the presence of remnant ice sheets, the initial conditions of this simulation are very different from the other simulations. In this simulation global mean sea level and vegetation cover have been fixed to pre-industrial values.

2.1.2 CCSM3

The CCSM3 (Community Climate System Model, version 3) GCM is a state-of-the-art global climate model composed of four separate components representing atmosphere (CAM3), ocean (POP), land, and sea-ice (Collins et al., 2006). Here, we use the low-resolution (T31 truncation in the atmosphere, nominal 3° resolution in the ocean) version of CCSM3 which is described in detail by Yeager et al. (2006). In this 130–115 ka BP simulation, global sea level, vegetation and ice sheet configuration have been fixed to modern values. Starting from a 130 ka BP equilibrium state, the transient simulation has been carried out with a 10 times accelerated astronomical forcing (as in the KCM simulation, see below) such that 15 000 yr are represented by a 1500 yr

CPD
8, 4663–4699, 2012

simulation. Note that the CCSM3 temperatures presented in this manuscript are radiative surface temperatures not near surface air temperatures. However, since we only analyse temperature anomalies the impact will be minor.

2.1.3 CLIMBER-2

The CLIMBER-2 EMIC is a so-called 2.5-D atmosphere-ocean-vegetation model of intermediate complexity (Petoukhov et al., 2000). The atmospheric component is a low resolution, 2.5-D statistical-dynamic model. The ocean model is a zonally-averaged multi-basin (Atlantic, Indian and Pacific) model which resolves these basins only in the latitudinal direction. CLIMBER-2 includes a thermodynamic sea-ice model that computes the evolution of sea-ice coverage and thickness. In this simulation global mean sea level and ice sheet configuration have been fixed to pre-industrial values. However, vegetation is actively simulated. This transient simulation is part of a longer simulation covering the last 4 glacial-interglacial cycles (420–0 ka BP) making the initial conditions of this simulation different from the other simulations used in this inter-comparison study.

2.1.4 FAMOUS

The FAMOUS GCM (Jones et al., 2005; Smith et al., 2008; Smith and Gregory, 2012) is a low resolution version of the HadCM3 GCM (Gordon et al., 2000) with roughly half the horizontal resolution of HadCM3 in both the atmosphere and ocean and a longer time-step. In this transient LIG simulation a fixed, pre-industrial global mean sea level, vegetation cover and ice sheet configuration is prescribed. The simulation was spun up with a 2000-yr long transient run for the period of 132–130 ka BP, including changes in the astronomical configuration and GHG concentrations. Note that this spin-up procedure is according to the PMIP3 protocol (http://pmip3.lsce.ipsl.fr).

CPD
8, 4663–4699, 2012

2.1.5 Kiel Climate Model

The Kiel Climate Model (KCM) GCM consists of the ECHAM5 atmospheric GCM coupled to the Nucleus for European Modeling of the Ocean (NEMO) ocean-sea-ice GCM (Park et al., 2009). Global mean sea level, vegetation cover and ice sheet configuration are fixed to pre-industrial values. The simulation runs from 126 to 115 ka BP starting from a 126 ka BP equilibrium state. The simulation has been performed with a 10 fold acceleration of the changes in the insolation forcing. In other words, an 1100 yr simulation is taken to represent the full 126–115 ka BP period.

2.1.6 LOVECLIM

The LOVECLIM EMIC includes a simplified atmospheric component and a low resolution ocean GCM (Goosse et al., 2010). In this transient LIG simulation, global mean sea level, vegetation cover and ice sheet configuration are fixed to pre-industrial values. The simulation was spun up with a 2000 yr long transient run for the period of 132–130 ka BP, including changes in the astronomical configuration and GHG concentrations. Note that this spin up procedure is according to the PMIP3 protocol (http://pmip3.lsce.ipsl.fr) and is identical to the one used for the FAMOUS simulation.

2.2 Data processing

All the simulated temperature fields were averaged into 50-yr averages for every month. For the CCSM3 and KCM simulations, which are performed with a 10 fold acceleration of the changes in the insolation forcing, averaging over 50 astronomical years effectively means an average over only 5 model years. These differences mean that the degree to which short time-scale climate variability is filtered out differs from sub-decadal (CCSM3 and KCM) to multi-decadal (all other models). We note that the results in the two accelerated simulations (CCSM3 and KCM) will be affected by the sluggish nature of the oceans, but deem this of minor importance (Lorenz et al., 2004). In order to

CPD
8, 4663–4699, 2012

smooth out the artificial noise resulting from the fact that the MPI-UW model was integrated in periodically-synchronous mode the temperature series have been averaged using a 200 yr window and afterward linearly interpolated to obtain 50 yr averages. All outputs of the different simulations were linearly re-gridded onto a common rectangular 1° × 1° grid. Throughout this manuscript, when dealing with 'temperatures' we refer to near surface air temperature anomalies (i.e. differences between simulated LIG and pre-industrial surface air temperatures). The pre-industrial temperatures were obtained by averaging over the last 30–100 yr of long (> 500 yr) equilibrium simulations with pre-industrial values for the orbital parameters and GHG concentrations (see also http://pmip3.lsce.ipsl.fr).

2.3 Evolution of the main climatic forcings of the LIG period

In order to investigate the LIG temperature evolution it is important to have an overview of the changes in two of the main climate forcings: the amount of insolation received by the Earth and atmospheric GHG concentrations. The changes in insolation and GHG concentrations are plotted in Figs. 1 and 2 (values according to the PMIP3 protocol, http://pmip3.lsce.ipsl.fr/). The insolation anomalies shown in Fig. 2 are given for the middle latitude of the latitudinal band under consideration and for a set of months, namely December, January, February (DJF) and June, July, August (JJA). Comparing the simulated temperature anomalies with the the insolation changes for different months and the changes in GHG concentrations, allows us to relate the temperature evolution to a given forcing. We will also identify which of the simulated temperature trends are not directly connected to changes in the insolation or GHG concentrations, and therefore possibly result from internal feedback mechanisms.

The changes in the amount of insolation received by the Earth result from changes in the astronomical configuration. Globally averaged, the anomalies are close to zero for the LIG period. However, changes in the distribution over the different latitudes and seasons are not. During the first part of the LIG, the NH received more insolation in summer (JJA) compared to the present-day period. Differences in insolation

CPD
8, 4663–4699, 2012

between both periods exceed 70 W m^{-2} for June at 75° N (~ 130–122 ka BP with a peak around ~ 127 ka BP; Fig. 2). Note that the maximum insolation anomaly did not occur during the same period for all summer months. For instance, the August insolation maximum occurred around 7 ka later (~ 120 ka BP) than the June maximum. The trend in NH winter insolation (DJF) is rather different. At high latitudes (>~ 67° N), absolute insolation and the insolation anomalies are close to zero in boreal winter. In the mid-latitudes of the NH, a minimum is observed during the first half of the LIG (~ 127–124 ka BP) in the winter months, while maximum values are found at the very end of the LIG (< 116 ka BP). In the equatorial region the changes in insolation are similar to the ones described for the rest of the NH although the magnitude of the early LIG DJF minimum is now larger than the JJA maximum. For the Southern Hemisphere (SH) summer (DJF), the changes in insolation show a strong minimum between 126–123 ka BP while insolation values are just above the present-day ones during the late LIG (< 118 ka BP). For the SH winter season (JJA) at 45° S, the maximum is between 127–125 ka BP. Again, in the high-latitudes, south of ~ 67° S, JJA insolation anomalies were close to zero.

While all simulations in this model inter-comparison include changes in the astronomical configuration, only some include changes in GHG concentrations. The FAMOUS and LOVECLIM simulations include changes in CO_2, CH_4 and N_2O, the Bern3D simulation includes changes in CO_2, CH_4 and the CLIMBER-2 simulation only includes changes in CO_2 (all values in accordance with the PMIP3 protocol). The GHG concentration values for the LIG period in the PMIP3 protocol are based on ice-core data of Luthi et al. (2008), Loulergue et al. (2008) and Schilt et al. (2010) for respectively CO_2, CH_4 and N_2O. A linear interpolation was applied to these data in order to get either a 100 yr (CLIMBER-2 and FAMOUS) or a 1 yr (Bern3D and LOVECLIM) time-resolution. In contrast to insolation changes, GHG concentrations are spatially homogenous on the time-scales of interest (multi-decadal to millennial). The concentrations show a strong increase from low, values around 130 ka BP towards high values at 128 ka BP (Fig. 1). The peak in CO_2 concentrations around 128.5 ka BP is sharp and short lived

CPD
8, 4663–4699, 2012

(i.e. centennial time scale). It reaches values above 280 ppm around 128.5 ka,BP, after which values fluctuate around 270 ppm until the end of the simulations period at 115 ka BP. The evolution of CH_4 concentrations shows an almost linear decline from 128 ka to 115 ka BP while the trend in the N_2O concentration is rather similar to the trend found for CO_2. Note that the radiative forcing provided by the changes in the three major GHGs is only small, $< 0.2\,W\,m^{-2}$, compared to the forcing provided by the insolation changes (Fig. 1). The KCM and CCSM3 simulations have GHG concentrations fixed at pre-industrial and 'average LIG' values respectively (average LIG here means: 272 ppm CO_2, 622 ppb CH_4 and 259 ppb N_2O). In the simulation performed with the MPI-UW model, the pCO_2 concentration is a prognostic variable. Therefore the evolution of the GHG forcing in the MPI-UW simulation (CO_2 only, CH_4 and N_2O are neglected) is different from the other simulations (Fig. 1). The simulated GHG evolution in the MPI-UW simulation is characterized by a slow increase between 128–122 ka BP from $\sim$ 270 ppm towards more stable values of around 285 ppm between 122–115 ka BP. In all the simulations described in this study, a fixed-day calendar is used. Although this will quantitatively affect the results, especially for the late summer months (Chen et al., 2011), the impact is of minor importance when we consider the robustness of the simulated temporal evolution of LIG temperatures and the differences between the different simulations (Joussaume and Braconnot, 1997).

3 Results: simulated LIG temperature evolution

Because of the seasonal and latitudinal differences in insolation, we investigate the simulated evolution of LIG temperature anomalies for both January and July in 5 different latitude bands: high-northern latitudes, mid-northern latitudes, the tropical region and the mid and high-southern latitudes (respectively 60° N–90° N; 30° N–60° N; 30° S–30° N; 60° S–30° S and 90° S–60° S). These specific latitudinal bands were chosen because some important feedbacks of the climate system are roughly confined to these latitudinal bands, e.g. the albedo and sea-ice feedback in the higher latitudes and the

CPD
8, 4663–4699, 2012

monsoon system in the equatorial latitudes. With this approach we explicitly assume that longitudinal differences in temperature anomalies are small compared to latitudinal differences. Spatial patterns in the evolution of surface temperature anomalies will be investigated to test the validity of this assumption. We focus here on January and July temperatures to investigate changes in either the cold or warm season. However, we do note that these months do not always represent the warmest or coldest months for a given location.

For most latitudinal bands and for both January and July, a robust temperature anomaly trend is simulated by the different models. The overall trend and its robustness are illustrated by the multi-model-mean (MMM) and the accompanying standard deviation (STDEV; Fig. 2).

In the mid and high-latitudes of the NH we find peak July temperature anomalies of 0.4–6.8 K compared to pre-industrial between ~ 130–122 ka BP. The resulting MMM trend has a relatively small STDEV and is in line with June insolation changes and the evolution of the radiative forcing resulting from the GHG concentration changes. Simulated January temperature anomalies for the NH mid-latitudinal band show a rising trend and a 0–2 K peak between ~ 122–115 ka BP. These simulated January temperatures are in line with December insolation changes. The exceptions are in the FAMOUS simulation which shows a clear 2.5 K peak at 121 ka BP and the MPI-UW simulation which does not show a clear peak. For the high-latitudes of the NH, no robust January trend is found when comparing the different simulations. Four out of seven simulations show peak warmth around ~ 120 ka BP but in CCSM3, LOVECLIM and MPI-UW it is found before ~ 122 ka BP. The most striking feature in the simulated January temperatures in the high-latitudes of the NH is the large offset between the different models, with average temperature anomalies ranging from ~ −7 K (CCSM3) to ~ +2 K (FAMOUS) which results in the large STDEV depicted in Fig. 2.

In the latitudinal band of the tropical region we find a robust trend in simulated January temperature anomalies with a peak of 0.8–1.5 K after ~ 121 ka BP. This is in line with the evolution of December insolation. For July the simulated temperature changes

CPD
8, 4663–4699, 2012

in the tropical region are less robust. All models simulate peak warmth between ~ 130–124 ka BP in line with changes in June insolation and GHG concentrations. However, during the first half of the interglacial period the STDEV is rather large, with a 0–2.9 K range of peak temperature anomalies, while it is much smaller during the later half.

In the mid-latitudes of the SH we find a relatively robust evolution of January temperature anomalies. Peak anomalies of 0.3–2 K are simulated between ~ 121–115 ka BP in accordance with December insolation. Furthermore, all simulations which include changes in GHG concentrations according to the PMIP3 protocol simulate a second peak of smaller magnitude between 129–128 ka BP in line with the GHG forcing. January temperature anomalies in the mid-latitudes of the SH simulated by the MPI-UW model, are charecterized by large, ~ 1 K fluctuations. The simulated January temperature anomalies for the high-latitudes of the SH show a similar pattern as described for the mid-latitudes with again a peak after 121 ka BP. However, the MPI-UW simulation does not show this trend and the signal seems rather dominated by the same high-frequency variability described for the mid-latitudes of the SH. Another noticeable difference is the ~ –3 K offset in the temperature anomalies simulated by the LOVECLIM model. For July in the SH (winter in this hemisphere) no robust temperature trend is found. For both the mid and high-latitudes, the simulations including changes in GHG concentrations according to the PMIP3 protocol show maximum warmth between ~ 129–124 ka BP. However, the magnitude of the overall trend is small compared to the size of the STDEV. Again the MPI-UW temperature evolution is dominated by large, up to 6 K high-frequency variability.

To conclude, the different simulations show overall agreement on the simulated trends in January and July temperature anomalies for most of the latitudinal bands. In the NH, maximum summer (July) temperatures were reached before 125 ka BP while winter (January) temperatures peaked after 122 ka BP. The forcings for the SH are very similar to the NH when the timing of the radiative maximum is concerned and in line with this we find a very similar evolution of simulated January and July temperatures. Consequently we find that summer and winter temperatures in the SH peaked after

CPD
8, 4663–4699, 2012

~ 121 ka BP and before 124 ka BP respectively. Only for January in the 60° N–90° N latitudinal band and in the mid to high-latitudes of the SH, no robust temperature evolution is simulated.

These findings, combined with the trends in the radiative forcings, indicate that simulated January and July surface temperature anomalies are mostly in line with respectively December and June insolation. Furthermore we see that when the rate of change of the radiative forcing is large, the model results are robust but without a strong trend in the radiative forcing the resulting temperature evolution tends to be very different. The latter case is especially true for the simulated temperature trends in the winter months in high latitude regions which are characterized by a very small insolation forcing. Simulated July temperature anomalies for the SH exemplify another finding. Namely, we see that the simulations that include changes in GHG concentrations tend to simulate a more distinct evolution of surface air temperature compared to the models that have fixed GHG concentrations (CCSM3 and KCM). This highlights that the radiative forcing provided by the changes in GHG concentrations is important, though mainly when the magnitude and trend in the insolation forcing is small. However, the impact of the different GHG forcing evolution applied in the MPI-UW simulation is not easily identified.

Lastly we investigate the impact of differences in the model complexity and model resolution on the simulated temperature evolutions. The results show that we can conclude that on longer (> 1 ka) timescales and large spatial-scales (latitudinal bands for instance) the differences between EMICs and GCMs are of minor importance. However, the simulated high-frequency climate variability (50–100 yr timescales in this study because of the applied time-averaging) is much larger in the models of higher complexity and resolution. Furthermore, including a coupled dynamical terrestrial biosphere component to the model as in the MPI-UW simulation, causes the temperatures in the mid to high-latitudes of the NH to be higher compared to most other models because of the positive vegetation-albedo feedback (Schurgers et al., 2007).

CPD
8, 4663–4699, 2012

Even though we found many robust trends in simulated temperature evolutions, there are some interesting differences which we will discuss in the next section.

4 Discussion

Comparing the results of different climate simulations enables us to investigate the robustness of the simulated LIG temperature evolution. These results can then be used to improve our understanding and interpretation of the climatic signal provided by different proxy-based climate reconstructions. Moreover, the differences between the simulations and specific spatial patterns in the simulated temperature changes can provide valuable information about the functioning of climate system during the LIG. Even though an in-depth investigation of the causes of these inter-model differences and spatial patterns is outside the scope of this manuscript, we will list the most apparent ones and present a first interpretation in terms of climate feedbacks.

While the astronomical and GHG forcings are longitudinally homogeneous, the net effect of insolation changes and feedback mechanisms within the climate system can result in longitudinal differences in the temperature evolution. To investigate the importance of feedback mechanisms we focus on the MWT for different months. The MWT has been calculated by taking the maximum 50-yr average temperature for each individual model.

Figure 3 clearly shows that there are longitudinal differences in the MWT in January and July. Furthermore, in some models there are also latitudinal differences within the specified latitudinal bands. However, interpreting these results is difficult since there are many potential causes: differences in the internal climate feedbacks, included forcings, model-physics, parameterizations and model-resolution. Therefore, we have calculated the MMM and STDEV of the MWT which we use to characterize the overall trend in the different simulations and the level of agreement between them. In this case we do not only look into January and July temperatures but to all winter and summer months (DJF and JJA; Fig. 4). This allows for a more thorough investigation of regional and

CPD
8, 4663–4699, 2012

longitudinal differences in the simulated LIG MWT for a specific month which we will attempt to link to specific feedback mechanisms.

4.1 Sea-ice and the LIG temperature evolution

For the Arctic Ocean, we find overall agreement on an early, >∼ 123 ka BP, MWT in DJF. During DJF the insolation forcing is close to zero in the Arctic, however the early warming is in line with the peak in the radiative forcing resulting from the changes in GHG concentrations according to the PMIP3 protocol. However, the presence of sea ice in the Arctic Ocean provides a strong positive feedback within the climate system. It seems that, in line with findings for the Holocene (Renssen et al., 2005), the early LIG June insolation maximum results in a decline in the summer sea-ice cover and thickness and a consequent decline in the winter sea-ice cover and thickness. This could in turn enhance the heat-flux from the ocean to the atmosphere leading to higher atmospheric winter temperatures. The relative importance of either the GHG forcing or the sea-ice feedback on the Arctic winter MWT is not easily determined. However, 2 out of 3 simulations not including an early LIG GHG maximum (CCSM3 and MPI-UW) do show an early DJF temperature optimum over the Arctic. Furthermore, it is apparent that the early January temperature maximum is mainly found over the Arctic Ocean, the only region in the NH where extensive sea-ice is present. Both findings provide strong indications that the sea-ice feedback plays an important role in determining the LIG winter temperature evolution in the Arctic region.

Interestingly, the situation in the sea-ice covered regions surrounding Antarctica is rather different. In contrast to the Arctic Ocean, in most simulations the MWT in DJF and JJA for the sea-ice covered areas of the SH summer do not coincide. Rather, the winter (JJA) MWT in these areas is ∼ 127 ka BP while the summer (DJF) MWT is after ∼ 120 ka BP. Note, that while in the Arctic the peak in summer insolation and the peak in the GHG forcings coincide (∼ 128 ka BP), this is not the case in the Antarctic region. Furthermore, in several of the simulations, namely those performed with CCSM3, KCM

CPD
8, 4663–4699, 2012

and MPI-UW, especially large variability is simulated in high-latitude SH July temperatures which might involve changes in the sea-ice cover over the Southern Ocean.

All these findings highlight the need for a more thorough investigation to establish the importance of sea-ice cover changes for the evolution of LIG temperatures in high-latitude regions in general, and the possible differences between the Arctic and Antarctic regions.

4.2 The AMOC and the LIG temperature evolution

Several of the simulations in this inter-comparison study show large, abrupt changes in surface temperature anomalies that are not easily related to changes in the forcings.

For instance, the FAMOUS model simulates an abrupt decline in January temperatures in the NH around 121 ka BP, followed within centuries by an abrupt increase of January and July temperatures at mid-southern latitudes. Furthermore, the FAMOUS simulation shows an anomalous MWT pattern over the Southern Ocean and over the northern and north-eastern Pacific in January (Fig. 3). The simulation performed with LOVECLIM also shows an abrupt January cooling at around 120 ka BP (Fig. 2). Accompanying this temperature shift is a region of anomalous timing of winter warmth in the Labrador Sea (Fig. 3). The Bern3D model shows a similar anomalous spatial pattern over the Labrador Sea with a timing of maximum winter warmth clearly offset from the surrounding areas. The last model simulating abrupt changes in the temperature time-series is CLIMBER-2. In the period between 123–120 ka BP, we see large fluctuations with a duration of about 1 ka.

In all four simulations these abrupt changes are related to changes in the AMOC. We conclude this by comparing their timing with the evolution of the AMOC (Fig. 5). The strength of the AMOC has a large impact on the oceanic heat transport from the tropics to the high latitudes and the exchange of heat between the SH and NH. Furthermore, it has a large impact on the heat exchange between the atmosphere and the ocean. The strength of the AMOC can change rapidly because of its potentially bi-stable behaviour (Stommel, 1961). However, the strength, stability and the locations

CPD
8, 4663–4699, 2012

of the main convective regions are highly model-dependent. As a result, the simulated LIG evolution of AMOC characteristics differs largely between the various models.

The LIG simulation performed with the FAMOUS model is characterized by two different modes of the AMOC. Between 120 ka and 115 ka BP a strong AMOC is simulated (Fig. 5) which is characterized by deep convection mainly taking place in the North Atlantic. Between 130–121 ka BP a different mode of the AMOC is simulated which is characterized by a strongly weakened AMOC (~ 70 % weaker compared to the strong mode of the AMOC; Fig. 5) and a shift of deep convection from the North Atlantic to the North Pacific (not shown). The change in the mode of the AMOC around 121 ka BP is related to the simulated temperature changes around 121 ka BP (Fig. 2) and the anomalous MWT in the Southern Ocean and parts of the North Pacific (Figs. 3 and 4). However, an explanation of the NH January temperature fluctuations depicted in Fig. 2 is complicated by the fact that they are longitudinal averages which thus encompass both the North Atlantic and the North Pacific. Therefore, changes in deep convection and associated heat release to the atmosphere in these regions may partly compensate each other. Furthermore, it seems that changes in the sea-ice cover and the dynamics of the Southern Ocean play an important role in the simulated climatic changes around 121 ka BP (not shown).

Another model simulating changes in the AMOC is the Bern3D model. As mentioned before, the Bern3D model incorporates both prescribed remnant ice sheets and a related meltwater flux entering into the ocean between roughly 130–125 ka BP (see Sect. 2.1.1). Concurrent with this melt flux, a somewhat weakened (–20–30 %) AMOC is simulated for the period 129–125 ka BP (Fig. 5). After 121 ka BP, growth of the NH continental ice sheets is prescribed in the Bern3D simulation. To compensate for this, a volume of freshwater is removed globally from the surface of the ocean. Therefore the surface ocean densifies and as a result an increase of the AMOC strength is simulated (not shown). Note however, that this AMOC strengthening does not seem to have a clear impact on the simulated LIG temperature evolution (Fig. 2).

CPD
8, 4663–4699, 2012

The strength of the AMOC in the CLIMBER-2 simulation shows apparent shifts in the 123–120 ka BP period (Fig. 5). Interestingly, while the changes in AMOC strength are less than 10 %, they cause major, ∼ 4 K shifts in the temperature of the mid-latitudes of the NH. This could also indicate that other climate feedbacks cause the simulated temperature fluctuations which in turn cause the changes in AMOC strength.

The fourth simulation with changes in AMOC strength is the LOVECLIM simulation. Around 120 ka BP, the AMOC weakens abrupt by about 15 % and remains unstable thereafter. The simulated changes in AMOC strength in the LOVECLIM model are related to periods of weakened convection in the Irminger Sea (not shown here). Two quasi-stable AMOC modes have already been described for the LOVECLIM model by Schulz et al. (2007). An interesting question is if the mode transitions in the FAMOUS and LOVECLIM simulations are determined by an external forcing or that they occur by chance (stochastically) at around 120 ka BP. Running the ensemble simulations necessary to answer this question is however outside the scope of the manuscript.

The simulations performed with the KCM and CCSM3 models show a more stable AMOC throughout the LIG. Finally, the MPI-UW simulation shows fluctuations (Fig. 5) related to multi-centennial variability in Southern Ocean deep convection caused by a limit-cycle which strongly affects the production of Antarctic Bottom Water (AABW; not shown). This mechanism is also related to the high-frequency variability in the SH visible in Fig. 2.

Regardless of the exact mechanisms causing the changes in the AMOC in the different simulations, which is outside the scope of this manuscript, the results show the importance of the evolution of the configuration and strength of the AMOC for the simulated evolution of LIG temperature anomalies. This is especially true for regions like the Southern Ocean, the north-eastern Pacific, the North Atlantic, the Labrador Sea, the Norwegian and the Barents Sea.

In order to simulate a more robust LIG temperature evolution for these regions, stronger constraints are needed on how the configuration of the AMOC evolved and

CPD
8, 4663–4699, 2012

if mode-switches occurred during the LIG which is, to date, still inconclusive (Nieuwenhove et al., 2011).

4.3 Ice sheets and the LIG temperature evolution

In the transient LIG simulation performed with the Bern3D model, changes in the size of the continental NH ice sheets were prescribed. According to the method applied by Ritz et al. (2011a) to reconstruct remnant ice sheets, parts of the NH continents remained glaciated until ~ 125 ka BP (see Sect. 2.1.1). Therefore, this simulation provides the possibility to investigate the possible impact of remnant ice sheets on the LIG temperature evolution. The impact of remnant ice seems most clearly visible in the simulated July temperature evolution in high-northern latitudes. The peak warmth simulated by the Bern3D model occurs several thousands of years later than in most of the other simulations (Fig. 2). Furthermore, Fig. 3 shows that in this simulation, July maximum warming seems not only delayed in mid to high-northern latitudes but also in mid and high-latitudes of the SH. Note however, that it is not easy to distinguish between the impact of remnant ice or the weakening of the AMOC.

For the present interglacial period, Renssen et al. (2009) have shown that remnant ice sheets had a profound influence on the surrounding regions, delaying the thermal maximum to several thousands of years after the insolation optimum. The simulation performed with the Bern3D model, even though of lower resolution than the model used by Renssen et al. (2009), indicates a similar delay of maximum warmth. However, a thorough comparison of several simulations including remnant ice sheets is needed to retrieve a more robust signal of the impact of remnant ice on the LIG temperature evolution. Such a model inter-comparison is however further complicated by the fact that different reconstructions of the changes in altitude and extent of the ice sheets during the LIG are still inconclusive. According to Kopp et al. (2009), maximum LIG sea-level was at least 6 m above present-day. A small part of this can be accounted for through thermal expansion of the ocean waters (McKay et al., 2011) and a loss of mountain glaciers. But the magnitude of volume loss from the Greenland Ice Sheet

CPD
8, 4663–4699, 2012

and if a substancial contribution from the Antarctic Ice Sheet is required is still heavily debated (Dutton and Lambeck, 2012, and references therein).

4.4 The monsoon and the simulated LIG temperature evolution

Finally we will discuss the anomalous pattern in simulated LIG temperatures in the Sahel region and in India. In the JJA months, the simulated MMM MWT over these regions is clearly later then the surrounding regions (Fig. 4). However the large STDEV value shows that this anomalous pattern is only simulated by some of the models. Maximum July temperatures over the Sahel and India are reached before 126 ka BP in Bern3D and LOVECLIM, around 124 ka BP in CLIMBER-2 and after 120 ka BP in CCSM3, KCM and MPI-UW. Again another pattern is simulated by the FAMOUS model, showing an early (> 128 ka BP) MWT over the Sahel but a late (< 118 ka BP) MWT over parts of India (Fig. 3). Solely based on the geographical distribution of these anomalous temperature patterns, we relate them to changes in the monsoon system. There are several important differences between the different models which can at least partly explain the large STDEV in these areas. The GCMs in this model inter-comparison (CCSM3, KCM and MPI-UW) simulate a MWT in the Indian and African monsoon regions which is delayed with respect to the insolation forcing. This can be explained by strong feedbacks between the insolation, land evapotranspiration and cloudiness as described by e.g. Mulitza et al. (2008). In the MPI-UW simulation this negative feedback related to clouds and precipitation is partly compensated by the positive vegetation-albedo feedback in these regions as savanna is partly replaced by tropical and temperate forests (not shown). The EMICs in this model inter-comparison have difficulty to realistically simulate changes in the monsoon system, probably because of their low resolution and simplified atmospheric physics and dynamics. For instance in the Bern3D model, the moisture transport is driven by fixed, zonally averaged winds which inhibit any changes in the monsoon system to be simulated. In LOVECLIM, the simulated changes in the equatorial region should also be treated with care since the results are strongly affected by the quasi-geostrophic nature of its atmosphere and the fixed cloud cover.

CPD
8, 4663–4699, 2012

Nonetheless, even though the exact climate change mechanisms at work for these specific regions are likely different in the different simulations and outside the scope of this manuscript, this model inter-comparison shows the importance of changes in monsoon systems for the evolution of LIG temperatures in regions like the Sahel and India.

4.5 Land-Sea contrasts

From Fig. 4 it becomes apparent that the simulated temperature evolution differs between the ocean and the adjacent landmasses. Throughout a seasonal cycle, maximum summer temperatures over the continents are reached in June and December for respectively the NH and the SH but the thermal inertia of the oceans causes the summer temperature maximum over the oceans to occur during respectively August and February. The difference between either June and August or between December and February in the timing of the LIG insolation maximum can be substantial, for instance > 5 ka in the NH (Fig. 2). Such differences can be crucial when proxy-based temperature reconstruction from different realms of the climate system are to be compared.

When this seasonal lag is taken into account, a comparison between the simulated timing of the June (December) MMM MWT over land and the August (February) MMM MWT over the oceans for the NH (SH) shows that for almost all regions the ocean lags the continent by ~ 2 ka (Fig. 4). However, the land-sea contrast in the MWT in the individual simulations (not shown here) reveals that the comparison is often difficult since in many regions the spatial patterns of the MWT are very patchy because of small scale climatic features.

From the performed model inter-comparison, no clear land-sea temperature relation emerges. However, it is interesting to note that maximum summer temperatures over the oceans do seem to lag maximum summer temperatures over the continents. But a > 5 ka lag in the NH as would be suggested by the evolution of the insolation anomalies, is not simulated by any of the climate models in this inter-comparison.

CPD
8, 4663–4699, 2012

5 Conclusions

In this manuscript we have presented the first model inter-comparison study of long, > 10 ka transient simulations covering the LIG period with a total of seven different climate models. Despite the large differences between the different climate simulations, we have shown a robust evolution of LIG January and July surface air temperature anomalies compared to pre-industrial values for large parts of the globe. More specifically:

- Simulated summer (July) temperatures for the NH show a robust temperature maximum between 130–122 ka BP with a magnitude ranging from 0.4–6.8 K.
- The simulated peak winter (January) warmth is less robust for the NH. For mid-latitudes (30° N–60° N) we find 122–115 ka BP with a magnitude of 0–2 K but for the high-latitudes (60° N–90° N) the simulations are inconclusive on the temperature evolution.
- However, over the Arctic Ocean a very robust 128–126 ka BP timing of peak January warmth is simulated.
- Simulated July temperatures in the equatorial regions show a 0–2.9 K maximum between 130–124 ka BP.
- Simulated January temperatures in the equatorial regions show a 0.7–1.4 K maximum between 121 ka and 115 ka BP.
- The simulated January temperature evolution for the SH shows a robust temperature maximum after 120 ka BP with however a fairly broad range of corresponding peak temperatures of −2.5 K to ∼ 2 K.
- For the SH we find a 129–124 ka BP July temperature maximum of 0.5–2.6 K in the four simulations which include prescribed changes in GHG concentrations.

CPD
8, 4663–4699, 2012

The three simulations not including these prescribed changes do not show a clear trend.

– The impact of higher model-complexity and or resolution is of minor importance for the simulated temperature evolution over longer (> 1 ka) timescales and large spatial-scales.

Based on the differences between the simulations and the investigation of regional patterns in the timing of maximum warmth we found the following:

– The sea-ice feedback plays an important role in determining the simulated timing of maximum winter warmth in the Arctic Ocean. The role of the sea-ice feedback in the Antarctic region is less clear.

– Four out of seven simulations show changes in the strength and configuration of the AMOC and a concequent impact on the evolution of surface temperatures during the LIG.

– Prescribing remnants of NH continental ice sheets is shown to impact the simulated NH high-latitude LIG temperature evolution.

– Four out of seven simulations show anomalous patterns in the timing of maximum warmth in the Sahel region and/or India. These patterns are related to changes in the monsoon system which can thus, regionally, have a large influence on the evolution of LIG temperatures.

– A land-sea contrast in the timing of maximum summer temperatures is found with on average the ocean summer temperature maximum lagging the continental summer temperature maximum by ∼ 2 ka.

The results of the model inter-comparison presented here highlight that several climate feedbacks are of major importance when simulating the evolution of LIG temperatures. This will serve as the starting point for a number of sensitivity studies that will

CPD
8, 4663–4699, 2012

be performed to determine exactly how important these feedbacks are and to investigate the mechanisms behind them. Furthermore, a model-data comparison will be undertaken in the near future to assess how our findings compare with proxy-based LIG climate reconstruction.

Acknowledgements. This is Past4Future contribution no. 32. The research leading to these results has received funding from the European Union's Seventh Framework programme (FP7/2007–2013) under grant agreement no. 243908, "Past4Future. Climate change – Learning from the past climate". CCSM3 simulations were performed on the SGI Altix supercomputer of the Norddeutscher Verbund fuer Hoch- und Hoechstleistungsrechnen (HLRN). Furthermore, we would like to thank Bette Otto-Bliesner from the National Center for Atmospheric Research (Boulder, USA) for her helpful suggestions.

References

Bauch, H. A. and Kandiano, E. S.: Evidence for early warming and cooling in North Atlantic surface waters during the last interglacial, Paleoceanography, 22, PA1201, doi:10.1029/2005PA001252, 2007. 4666

Braconnot, P., Harrison, S. P., Kageyama, M., Bartlein, P. J., Masson-Delmotte, V., Abe-Ouchi, A., Otto-Bliesner, B., and Zhao, Y.: Evaluation of climate models using palaeoclimatic data, Nature Clim. Change, 2, 417–424, doi:10.1038/nclimate1456, 2012. 4666

Calov, R., Ganopolski, A., Claussen, M., Petoukhov, V., and Greve, R.: Transient simulation of the last glacial inception. Part I: glacial inception as a bifurcation in the climate system, Clim. Dynam., 24, 545–561, 2005. 4667

CAPE-members – Anderson, P., Bennike, O., Bigelow, N., Brigham-Grette, J., Duvall, M., Edwards, M., Fréchette, B., Funder, S., Johnsen, S., Knies, J., Koerner, R., Lozhkin, A., MacDonald, G., Marshall, S., Matthiessen, J., Miller, G., Montoya, M., Muhs, D., Otto-Bliesner, B., Overpeck, J., Reeh, N., Sejrup, H. P., Turner, C., and Velichko, A.: Last Interglacial Arctic warmth confirms polar amplification of climate change, Quaternary Sci. Rev., 25, 1383–1400, 10.1016/j.quascirev.2006.01.033, 2006. 4666

CPD
8, 4663–4699, 2012

Chen, G., Kutzbach, J.E., Gallimore, R., and Liu, Z.: Calendar effect on phase study in paleoclimate transient simulation with orbital forcing, Climate Dynamics, 37, 1949–1960, doi:10.1007/s00382-010-0944-6, 2011. 4674

Collins, W. D., Bitz, C. M., Blackmon, M. L., Bonan, G. B., Bretherton, C. S., Carton, J. A., Chang, P., Doney, S. C., Hack, J. J., Henderson, T. B., Kiehl, J. T., Large, W. G., McKenna, D. S., Santer, B. D., and Smith, R. D.: The Community Climate System Model Version 3 (CCSM3), J. Climate, 19, 2122–2143, doi:10.1175/JCLI3761.1, 2006. 4669

Crucifix, M. and Berger, A.: Simulation of ocean-ice sheet interactions during the last deglaciation, Paleoceanography, 17, 1054, doi:10.1029/2001PA000702, 2002. 4667

Dutton, A. and Lambeck, K.: Ice Volume and Sea Level During the Last Interglacial, Science, 337, 216–219, doi:10.1126/science.1205749, 2012. 4684

Edwards, N. R. and Marsh, R.: Uncertainties due to transport-parameter sensitivity in an efficient 3-D ocean-climate model, Clim. Dynam., 24, 415–433, doi:10.1007/s00382-004-0508-8, 2005. 4668

Goosse, H., Brovkin, V., Fichefet, T., Haarsma, R., Huybrechts, P., Jongma, J., Mouchet, A., Selten, F., Barriat, P.-Y., Campin, J.-M., Deleersnijder, E., Driesschaert, E., Goelzer, H., Janssens, I., Loutre, M.-F., Morales Maqueda, M. A., Opsteegh, T., Mathieu, P.-P., Munhoven, G., Pettersson, E. J., Renssen, H., Roche, D. M., Schaeffer, M., Tartinville, B., Timmermann, A., and Weber, S. L.: Description of the Earth system model of intermediate complexity LOVECLIM version 1.2, Geosci. Model Dev., 3, 603–633, doi:10.5194/gmd-3-603-2010, 2010. 4671

Gordon, C., Cooper, C., Senior, C. A., Banks, H., Gregory, J. M., Johns, T. C., Mitchell, J. F. B., and Wood, R. A.: The simulation of SST, sea ice extents and ocean heat transports in a version of the Hadley Centre coupled model without flux adjustments, Clim. Dynam., 16, 147–168, doi:10.1007/s003820050010, 2000. 4670

Govin, A., Braconnot, P., Capron, E., Cortijo, E., Duplessy, J.-C., Jansen, E., Labeyrie, L., Landais, A., Marti, O., Michel, E., Mosquet, E., Risebrobakken, B., Swingedouw, D., and Waelbroeck, C.: Persistent influence of ice sheet melting on high northern latitude climate during the early Last Interglacial, Clim. Past, 8, 483–507, doi:10.5194/cp-8-483-2012, 2012. 4666

Gröger, M., Maier-Reimer, E., Mikolajewicz, U., Schurgers, G., Vizcaéno, M., and Winguth, A.: Changes in the hydrological cycle, ocean circulation, and carbon/nutrient cycling during the

CPD
8, 4663–4699, 2012

last interglacial and glacial transition, Paleoceanography, doi:10.1029/2006PA001375, 2007. 4667
Houghton, J., Ding, Y., Griggs, D., Noguer, M., van der Linden, P., Dai, X., Maskell, K., and Johnson, C.: Climate Change 2001: The Scientific Basis, Contribution of Working Group I to the Third Assessment Report of the Intergovernmental Panel on Climate Change, Cambridge University Press, 2001. 4694
Jones, P. D. and Mann, M. E.: Climate over past millennia, Rev. Geophys., 42, RG2002, doi:10.1029/2003RG000143, 2002 4667
Jones, P. D., Gregory, J., Thorpe, R., Cox, P., Murphy, J., Sexton, D., and Valdes, P.: Systematic Optimisation and climate simulations of FAMOUS, a fast version of HadCM3, Clim. Dynam., 25, 189–204, doi:10.1007/s00382-005-0027-2, 2005 4670, 4693
Joussaume, S. and Braconnot, P.: Sensitivity of paleoclimate simulation results to season definitions, J. Geophys. Res., 102, 1943–1956, doi:10.1029/96JD01989, 1997. 4674
Kopp, R. E., Simons, F. J., Mitrovica, J. X., Maloof, A. C., and Oppenheimer, M.: Probabilistic assessment of sea level during the last interglacial stage, Nature, 462, 863–867, doi:10.1038/nature08686, 2009. 4683
Lisiecki, L. E. and Raymo, M. E.: A Pliocene-Pleistocene stack of 57 globally distributed benthic δ^{18}O records, Paleoceanography, 20, PA1003, doi:10.1029/2004PA001071, 2005. 4669
Lorenz, S. and Lohmann, G.: Acceleration technique for Milankovitch type forcing in a coupled atmosphere-ocean circulation model: method and application for the Holocene, Clim. Dynam., 23, 727–743, doi:10.1007/s00382-004-0469-y, 2004. 4671
Loulergue, L., Schilt, A., Spahni, R., Masson-Delmotte, V., Blunier, T., Lemieux, B., Barnola, J.-M., Raynaud, D., Stocker, T. F., and Chappellaz, J.: Orbital and millennial-scale features of atmospheric CH_4 over the past 800,000[thinsp]years, Nature, 453, 383–386, doi:10.1038/nature06950, 2008. 4673, 4694
Lunt, D. J., Abe-Ouchi, A., Bakker, P., Berger, A., Braconnot, P., Charbit, S., Fischer, N., Herold, N., Jungclaus, J. H., Khon, V. C., Krebs-Kanzow, U., Lohmann, G., Otto-Bliesner, B., Park, W., Pfeiffer, M., Prange, M., Rachmayani, R., Renssen, H., Rosenbloom, N., Schneider, B., Stone, E. J., Takahashi, K., Wei, W., and Yin, Q.: A multi-model assessment of last interglacial temperatures, Clim. Past Discuss., 8, 3657–3691, doi:10.5194/cpd-8-3657-2012, 2012. 4667
Luthi, D., Le Floch, M., Bereiter, B., Blunier, T., Barnola, J.-M., Siegenthaler, U., Raynaud, D., Jouzel, J., Fischer, H., Kawamura, K., and Stocker, T. F.: High-resolution carbon dioxide

CPD
8, 4663–4699, 2012

concentration record 650,000-800,000[thinsp]years before present, Nature, 453, 379–382, doi:10.1038/nature06949, 2008. 4673, 4694
McKay, N. P., Overpeck, J. T., and Otto-Bliesner, B. L.: The role of ocean thermal expansion in Last Interglacial sea level rise, Geophys. Res. Lett., 38, L14605, doi:10.1029/2011GL048280, 2011. 4666, 4683
Mikolajewicz, U., Gröger, M., Maier-Reimer, E., Schurgers, G., Vizcaíno, M., and Winguth, A.: Long-term effects of anthropogenic CO_2 emissions simulated with a complex earth system model, Clim. Dynam., 28, 599–633, doi:10.1007/s00382-006-0204-y, 2007. 4693
Montoya, M.: PALEOCLIMATE MODELING, The Last Interglacial, Elsevier, doi:10.1016/B0-44-452747-8/00033-8, 2007. 4667
Mulitza, S., Prange, M., Stuut, J., Zabel, M., von Dobeneck, T., Itambi, A. C., Nizou, J., Schulz, M., and Wefer, G.: Sahel megadroughts triggered by glacial slowdowns of Atlantic meridional overturning, Paleoceanography, 23, PA4206, doi:10.1029/2008PA001637, 2008. 4684
Müller, S. A., Joos, F., Edwards, N. R., and Stocker, T. F.: Water Mass Distribution and Ventilation Time Scales in a Cost-Efficient, Three-Dimensional Ocean Model, J. Climate, 19, 5479–5499, doi:10.1175/JCLI3911.1, 2006. 4668, 4693
Nieuwenhove, N., Bauch, H. A., Eynaud, F., Kandiano, E., Cortijo, E., and Turon, J.-L.: Evidence for delayed poleward expansion of North Atlantic surface waters during the last interglacial (MIS 5e), Quaternary Sci. Rev., 30, 934–946, 2011. 4666, 4683
Park, W., Keenlyside, N., Latif, M., Stroh, A., Redler, R., Roeckner, E., and Madec, G.: Tropical Pacific Climate and Its Response to Global Warming in the Kiel Climate Model, J. Climate, 22, 71–92, doi:10.1175/2008JCLI2261.1, 2009. 4671
Petoukhov, V., Ganopolski, A., Brovkin, V., Claussen, M., Eliseev, A., Kubatzki, C., and Rahmstorf, S.: CLIMBER-2: a climate system model of intermediate complexity. Part I: model description and performance for present climate, Clim. Dynam., 16, 1–17, doi:10.1007/PL00007919, 2000. 4670
Renssen, H., Goosse, H., and Fichefet, T.: Contrasting trends in North Atlantic deep-water formation in the Labrador Sea and Nordic Seas during the Holocene, Geophys. Res. Lett., 32, 1–4, 2005. 4679
Renssen, H., Seppa, H., Heiri, O., Roche, D. M., Goosse, H., and Fichefet, T.: The spatial and temporal complexity of the Holocene thermal maximum, Nat. Geosci., 2, 411–414, 2009. 4683

CPD
8, 4663–4699, 2012

Ritz, S. P., Stocker, T. F., and Joos, F.: A Coupled Dynamical Ocean-Energy Balance Atmosphere Model for Paleoclimate Studies, J. Climate, 24, 349–375, doi:10.1175/2010jcli3351.1, 2011a. 4667, 4668, 4669, 4683, 4693

Ritz, S. P., Stocker, T. F., and Severinghaus, J. P.: Noble gases as proxies of mean ocean temperature: sensitivity studies using a climate model of reduced complexity, Quaternary Sci. Rev., 30, 3728–3741, doi:10.1016/j.quascirev.2011.09.021, 2011b. 4668, 4669, 4693

Schilt, A., Baumgartner, M., Blunier, T., Schwander, J., Spahni, R., Fischer, H., and Stocker, T. F.: Glacial-interglacial and millennial-scale variations in the atmospheric nitrous oxide concentration during the last 800,000 years, Quaternary Sci. Rev., 29, 182–192, doi:10.1016/j.quascirev.2009.03.011, 2010. 4673, 4694

Schulz, M., Prange, M., and Klocker, A.: Low-frequency oscillations of the Atlantic Ocean meridional overturning circulation in a coupled climate model, Clim. Past, 3, 97–107, doi:10.5194/cp-3-97-2007, 2007. 4682

Schurgers, G., Mikolajewicz, U., Gröger, M., Maier-Reimer, E., Vizcaíno, M., and Winguth, A.: The effect of land surface changes on Eemian climate, Clim. Dynam., 29, 357–373, doi:10.1007/s00382-007-0237-x, 2007. 4677

Sirocko, F., Litt, T., Claussen, M., and Sánchez Goñi, M.: The Climate of Past Interglacials, Elsevier, Amsterdam, The Nethernlands, 1st Edn., 2006. 4667

Smith, R. and Gregory, J.: The last glacial cycle: transient simulations with an AOGCM, Clim. Dynam., 38, 1545–1559, doi:10.1007/s00382-011-1283-y, 2012. 4670, 4693

Smith, R. S., Gregory, J. M., and Osprey, A.: A description of the FAMOUS (version XDBUA) climate model and control run, Geosci. Model Dev., 1, 53–68, doi:10.5194/gmd-1-53-2008, 2008. 4670, 4693

Stommel, H.: Thermohaline Convection with Two Stable Regimes of Flow, Tellus, 13, 224–230, 1961. 4680

Turney, C. S. M. and Jones, R. T.: Does the Agulhas Current amplify global temperatures during super-interglacials?, J. Quaternary Sci., 25, 839–843, doi:10.1002/Jqs.1423, 2010. 4666

Waelbroeck, C., Frank, N., Jouzel, J., Parrenin, F., Masson-Delmotte, V., and Genty, D.: Transferring radiometric dating of the last interglacial sea level high stand to marine and ice core records, Earth Planet. Sc. Lett., 265, 183–194, doi:10.1016/j.epsl.2007.10.006, 2008. 4666

Yeager, S. G., Shields, C. A., Large, W. G., and Hack, J. J.: The low-resolution CCSM3, J. Climate, 19, 2545–2566, doi:10.1175/JCLI3744.1, 2006 4669

CPD
8, 4663–4699, 2012

Table 1. This table describes the main features of the climate models involved in this model inter-comparison. The used acronyms are Earth system model of intermediate complexity (EMIC), general circulation model (GCM), astronomical configuration (orb), astronomical acceleration with a factor of 10 (acc), greenhouse-gas concentrations (ghg) and prescribed changes in ice sheet configuration (ice).

Model name	Model complexity	Time range (ka BP)	Included forcings	Additional components	Forcings according to PMIP3 protocol	Resolution atmospheric component	Resolution oceanic component	Reference
Bern3D	EMIC	130–115	orb/ghg/ice	–	no	between 3.2° and 19.2° by 10° and 1 vert. layer	between 3.2° and 19.2° by 10° and 32 vert. layers	Edwards and Marsh (2005); Müller et al. (2006); Ritz et al. (2011a); Ritz et al. (2011b)
CCSM3	GCM	130–115	orb(acc)	–	no	3.75° by 3.75° (T31) and 26 vert. layers	3.6° by 1.6° and 25 vert. layers	Collins et al. (2006)
CLIMBER-2	EMIC	130–115	orb/ghg	vegetation	yes	10° by 51° and 1 vert. layer	10° and 11 vert. layers	Petoukhov et al. (2000)
FAMOUS	GCM	130–115	orb/ghg	–	yes	5° by 7.5° and 11 vert. layers	2.5° by 3.75° and 20 vert. layers	Gordon et al. (2000); Jones et al. (2005); Smith et al. (2008); Smith and Gregory (2012)
KCM	GCM	126–115	orb(acc)	–	no	3.75° by 3.75° (T31) and 19 vert. layers	0.5° by 1.3° and 31 vert. layers	Park et al. (2009)
LOVECLIM	EMIC	130–115	orb/ghg	–	yes	5.6° by 5.6° and 3 vert. layers	3° by 3° and 20 vert. layers	Goosse et al. (2010)
MPI-UW	GCM	128–115	orb/prognostic pCO_2	vegetation, marine carbon cycle and biogeochemistry	no	5.6° by 5.6° (T21) and 19 vert. layers	4° by 4° and 22 vert. layers	Gröger et al. (2007); Mikolajewicz et al. (2007)

CPD
8, 4663–4699, 2012

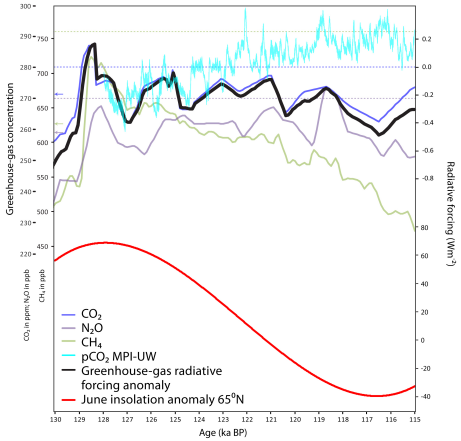

Fig. 1. In the upper part of the figure changes in the main GHG concentrations (CO_2, CH_4 and N_2O) over the period 130–115 ka BP are depicted. The corresponding pre-industrial values are given by the dotted lines. Concentrations are according to the PMIP3 protocol (http://pmip3.lsce.ipsl.fr/) which is based on the ice-core data of Luthi et al. (2008), Loulergue et al. (2008) and Schilt et al. (2010) for respectively CO_2, CH_4 and N_2O. In the simulations, a linear interpolation was applied to the data in order to get either 100 yr (FAMOUS and CLIMBER-2) or 1 yr (Bern3D and LOVECLIM) resolution. The bold black line presents the combined radiative forcing of the three main GHG concentration changes (W m^{-2}; concentrations according to the PMIP3 protocol; formulation of radiative forcing after Houghton et al., 2001). The fixed 'average LIG' GHG concentrations applied in the CCSM3 simulation are depicted by the arrows at the left-hand-side of the upper panel. In the MPI-UW simulation, the radiative forcing of the GHGs is prognostically calculated from simulated changes in the carbon cycle. The resulting CO_2 changes are depicted in light-blue. In the lower part of the figure the June insolation anomaly (W m^{-2}, compared to pre-industrial values) for 65° N is given.

CPD
8, 4663–4699, 2012

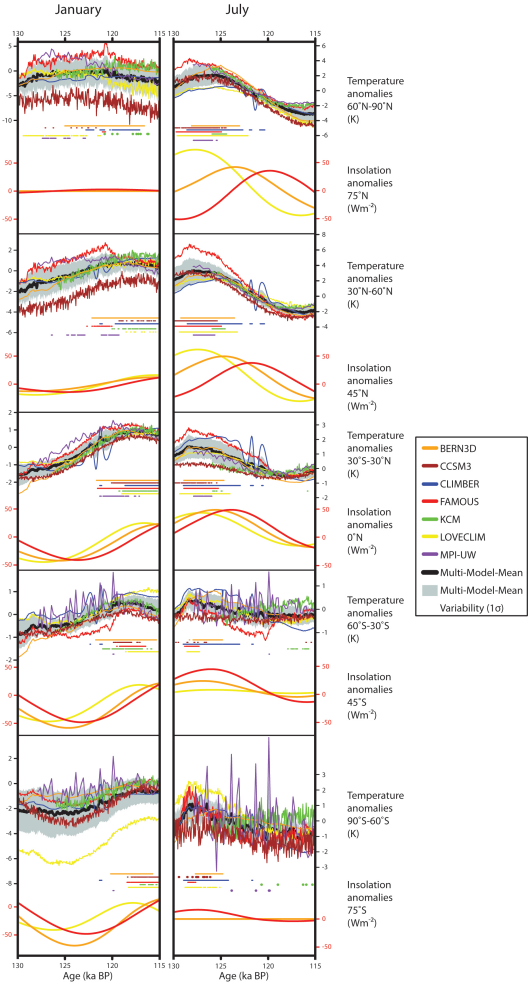

Fig. 2. Caption on next page.

CPD
8, 4663–4699, 2012

Fig. 2. Simulated 130–115 ka BP surface air temperature anomalies (K) for 5 different latitude bands and the according 130–115 ka BP insolation anomaly for the mid latitude of each latitudinal band (W m^{-2}). The left-hand column gives simulated January surface temperature anomalies and calculated December (yellow), January (orange) and February (red) insolation anomalies. The right-hand column gives simulated July surface air temperature anomalies and calculated June (yellow), July (orange) and August (red) insolation anomalies. All values are anomalies relative to pre-industrial values. The different models included are Bern3D (orange), CCSM3 (brown), Climber (blue), FAMOUS (red), KCM (green), LOVECLIM (yellow) and MPI-UW (purple). The temperature series are 50-yr averages. In black is depicted the multi-model-mean and in grey the standard deviation (68 % confidence interval; 1 σ). Note that for the period 130–128 ka BP, 128–126 ka BP and the period 126–115 ka BP the multi-model-means and standard deviations are based on respectively 5, 6 and 7 different simulations since the MPI-UW and KCM simulations run only from respectively 128–1115 ka BP and 126–115 ka BP. The horizontal bars accompanying the surface temperature anomalies are the periods of maximum warmth for each individual model. The length of this period is calculated by taking the maximum 50-yr average LIG temperature anomaly minus 20 % of the differences between the maximum and minimum value for each individual model. In all simulations shown in this figure a fixed-day calendar was used.

CPD
8, 4663–4699, 2012

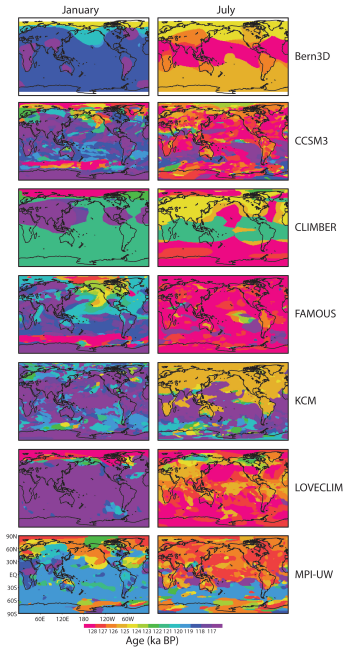

Fig. 3. Timing of the simulated LIG temperature maximum for the months January and July in the different simulations. The timing (ka BP) is calculated by taking the period for which the highest 50-yr average temperature anomalies are simulated. Note that Bern3D has latitudinal grid limits at 76° N and 76° S. Furthermore, the MPI-UW and KCM simulations run from 128–115 ka BP and 126–115 ka BP respectively, therefore the colour corresponding to a timing of respectively 128–127 ka BP and 126–125 ka BP should be interpreted as being > 127 ka BP or > 125 ka BP in case of the MPI-UW and KCM simulations. In all simulations shown in this figure a fixed-day calendar was used.

CPD
8, 4663–4699, 2012

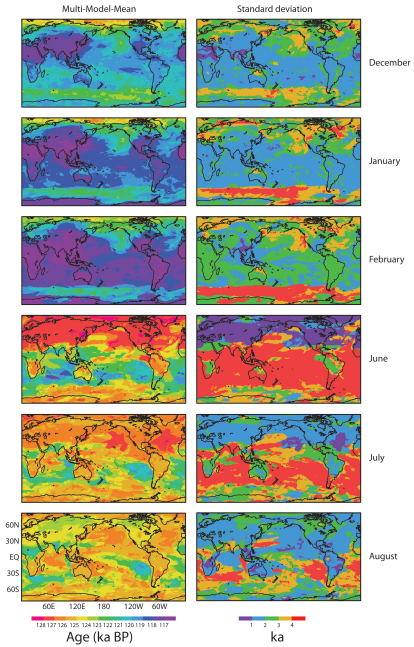

Fig. 4. Multi-model-mean (left) and standard deviation (right) of the timing of maximum warmth for 6 different months. The multi-model-mean of the timing of maximum warmth (ka BP) is calculated as the average over the timing of the 50-yr average period during which the highest temperatures have been simulated in the individual simulations. The standard deviation (ka) gives a measure of the spread in the simulated timing of maximum warmth between the different models. The calculations do not include the Bern3D model north of 76° N and south of 76° S in accordance with the Bern3D latitudinal grid limits. The calculations do include the KCM and MPI-UW simulations, however since they only run from 126–115 ka BP and 128–115 ka BP respectively, this might slightly offset the results shown in this figure. In all simulations shown in this figure a fixed-day calendar was used.

CPD
8, 4663–4699, 2012

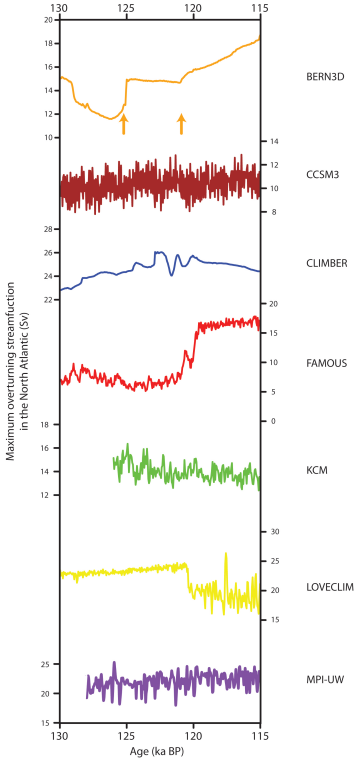

Fig. 5. Simulated LIG evolution of the strength of the AMOC in the seven different simulations. The maximum overturning streamfunction in the North Atlantic (Sv) is used to indicate the strength of the AMOC. All values are 50-(astronomical-)year averages. The arrows in the top panel indicate the moment when the meltwater flux from the remnant ice sheets into the oceans in the Bern3D simulation ceases (~ 125 ka BP) and when continental ice sheets on the NH start to form again (~ 121 ka BP).

CPD
8, 4663–4699, 2012